Electronic Supplementary Material (ESI) for Physical Chemistry Chemical Physics.

Supplementary Information: Temperature-dependent Li Vacancy Diffusion in $Li_4Ti_5O_{12}$ by Means of First Principles Molecular Dynamic Simulations

Pascal Henkel[a,b], Stefan Zahn[a,b,†], Janine Lorenz[a], Timo Jacob[c], Jürgen Janek[a,b] and Doreen Mollenhauer[a,b,#]

[a] Institute of Physical Chemistry, Justus-Liebig University Giessen, 35392 Giessen, Germany.

[b] Center for Materials Research (LaMa), Justus-Liebig University Giessen, 35392 Giessen, Germany

[c] Institute of Electrochemistry, Ulm University, Albert-Einstein-Allee 47, 89081 Ulm, Germany

[†] Current address: Leibniz Institute of Surface Engineering (IOM), Permoserstraße 15, 04318 Leipzig, Germany

[#] Corresponding author, Email: Doreen.Mollenhauer@phys.chemie.uni-giessen.de

S1: The Li vacancy localization method

As described in the main text, the localization of Li vacancies, even across supercell boundaries, is based on two approaches in two steps. The first approach is used to localize the Li vacancies and the second to characterize the corresponding diffusion steps.

First approach - localization of the Li vacancies: The location of each Li vacancy is analyzed based on the radial distribution function (RDF) in combination with a triangulation using the four or six under coordinated oxygen atoms. Due to the absence of a Li ion at a regular Li position (8*a* or 16*d*), a cavity is created in the Ti lattice of the LTO. Within these cavities, the RDF is minimal. Consequently, these cavities are identified in the first step. In this context, a simple $1/\boldsymbol{r}^3$-function is used to describe the RDF $\rho(\boldsymbol{r})$, with the distance vector $\boldsymbol{r}$ between any two ions. Moreover, the employed density function $\rho(\boldsymbol{r})$ ensures a fast decrease of the RDF within a cavity, which led to a precise localization of the Li vacancy positions. A 3D-mesh grid with a mesh spacing of $1/30 \cdot |a, b, c|$ (with a, b & c as lattice parameters) was applied to determine the RDF and $\rho(\boldsymbol{r})$ was calculated at each grid point. Periodic boundary conditions were taken into account by extending the system in each direction, leading to a system with a total of 27 unit cells, while the RDF was only determined in the center. Based on the chosen mesh spacing, which balances between the obtained accuracy and the computational effort, the resolution accuracy of the Li vacancy positions is $\sim$0.60 Å.

Due to the high simulation temperatures and the associated high lattice dynamic, several possible positions for the Li vacancy can be obtained. To determine the position of the Lithium vacancies more precisely the RDF was combined with a triangulation using the oxygen under-coordination. Thus the oxygen is not surrounded by four binding partners. The basis of this concept is that an unoccupied 8*a* or 16*d* position is surrounded by four or six under-coordinated oxygen ions. The oxygen under-coordination can be determined by the Ti-O and Li-O distances (we choose a maximum distance threshold of Ti-O: 2.35 Å and Li-O: 2.5 Å for this purpose). However, due to the high simulation temperatures, more than the expected 12 to a maximal 18 under-coordinated oxygens can be obtained from the vacancies (usually 12 - 20 under-coordinated oxygens out of 96 are determined). A reason for this is that the maximum distance is exceeded by the thermal motion and a regular coordinated oxygen (CN=4) can also appear as under-coordinated. The possible Li vacancy positions can be determined by triangulating 4 or 6 nearby under coordinated oxygen positions, but due to the large number of under-coordinated oxygen ions, more than three Li vacancy positions are possible.

Finally, the combination of the possible Li vacancy positions obtained by RDF and the oxygen under-coordination yield the final three vacancy positions. Then, the RDF is determined a second time, but starting from the obtained Li vacancy positions and only within a cube of ±2 Å in all three directions. This improves the resolution accuracy of the position to 0.17 Å. By performing this procedure for each time step, the positions of the Li vacancies are known at all times. The error rate is about 1 %. Approximately every 100 time steps, a Li vacancy position is incorrectly determined. In this way, the position of the Li vacancy is compared with its previous (known) position and correctly located in the following time step.

Second approach - characterization of diffusion steps: The characterization of the diffusion steps can be done by two approaches: a) directly via the Li vacancies or b) indirectly via the Li ions. In our study, we found that an indirect determination is much more accurate and is therefore used in this investigation. To determine the diffusion steps via the Li ions, first the 3-dimensonal (Cartesian) coordinates of each Li ion are projected to one axis, see Eq. (1);

$$\mathrm{F}_x[i][t] = x[i] + (y[i] \cdot |b|) + (z[i] \cdot |b| \cdot |c|) \qquad \text{(SI1)}$$

With $\mathrm{F}_x[i][t]$ as the projected dimension (on the x-axis) of the i-th Li ion at time t, which can be interpreted as a kind of motion amplitude. $x[i]$, $y[i]$ & $z[i]$ are the (Cartesian) coordinates of the i-th Li ion and b & c are the lattice parameters. A moving average filter is used to smooth the function $\mathrm{F}_x[i][t]$, eliminating minor artefacts and thermal noise. The diffusion steps can be characterized by plotting $\mathrm{F}_x[i][t]$ against t for each Li ion, see Fig.1.

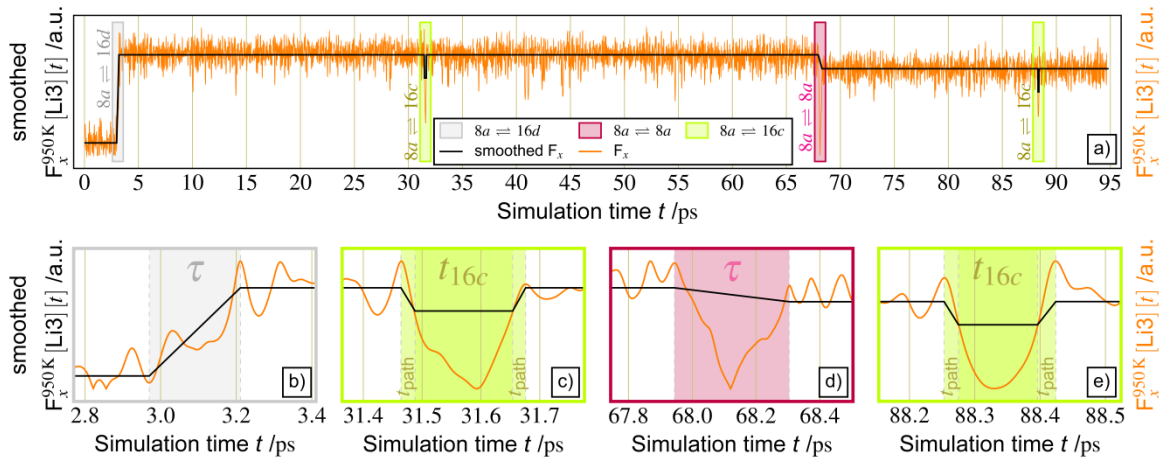

Figure S1: Original (orange) and smoothed (black) $F_x[i][t]$ function for the 3rd lithium ion (located at a 16*d* Wyckoff position initially) at a simulation temperature of 950 K. a) $F_x^{950\,\mathrm{K}}$[Li3][t] versus the total simulation time and zoomed ranges for each single diffusion steps in b) to e). b) 8*a*↔16*d*, c) first 8*a*↔16*c*, d) 8*a*↔8*a* and e) second 8*a*↔16*c* diffusion step. Lighter areas in figures b) - e) indicate the lifetimes of the transition sites. For the two 8*a*↔16*c* steps the actual lifetime t_{16c} and the two path times t_{path} can be determined, for the steps of 8*a*↔16*d* and 8*a*↔8*a*, only the lifetime τ can be determined (includes the true 16*c* lifetime t_{16c}, as well as path times t_{path} and for 8*a*↔16*d* the lifetime of the 48*f* site t_{48f}).

Using this method, the 8*a*↔8*a*, 8*a*↔16*c* and 8*a*↔16*d* diffusion steps can be distinguished and the lifetime τ of the transition sites of the Li ion can be determined (predominantly 16*c*). τ describes the lifetime needed for the Li ion to move from an 8*a* or 16*d* to a final/initial 8*a* or 16*d* Wyckoff position. The representation of $\mathrm{F}_x[i][t]$ can be used to distinguish the diffusion steps. Changes within $\mathrm{F}_x[i][t]$ indicate a diffusion step and depending on the intensity of the change, a distinction can be made between the three diffusion steps.

An 8*a*↔16*c* step is characterized by the formation of a plateau for a short time, see green ranges in Figs. S1c) and e). Thus, the steps 8*a*↔8*a* [see Fig. S1d)] and 8*a*↔16*d* [see Fig. S1b)] are characterized by a permanent change within the $\mathrm{F}_x[i][t]$ function. The change can be either increasing or decreasing depending on whether the step occurs beyond the boundary of the supercell. The difference between 8*a*↔8*a* and 8*a*↔16*d* diffusion paths is determined by the intensity of the change within $\mathrm{F}_x[i][t]$. The 8*a*↔16*d* diffusion step leads to a significant change in $\mathrm{F}_x[i][t]$ [see Fig. S1b)], while the change for the 8*a*↔8*a* diffusion step is less pronounced, see Fig. S1d). Instead of the moving average filter approach to determine the individual diffusion steps, an autocorrelation function approach could also be used. Thus, it is expected that similar results can be obtained. However, in this work, the moving average filter approach is used as an alternative.

The lifetime τ is composed of different contributions. For the 8*a*↔8*a* and 8*a*↔16*c* diffusion step, τ is composed by the 16*c* lifetime t_{16c} and the path time t_{path} required for the Li ion to move from an 8*a* to a 16*c* Wyckoff position (and *vice versa*). Thus, the lifetime is determined by: $\tau = t_{16c} + 2 \cdot t_{\mathrm{path}}$. In contrast, for the 8*a*↔16*d* diffusion step, τ is composed of three path times (between 8*a* and 16*c*, 16*c* and 48*f* and 48*f*, 16*d* as well as all reverse steps) and of the t_{16c} and t_{48f} lifetimes. Thus, the lifetime is determined by: $\tau = t_{16c} + t_{48f} + 3 \cdot t_{\mathrm{path}}$. However, t_{16c} cannot always be determined by using the $\mathrm{F}_x[i][t]$ function. In this case, the lifetime t_{16c} is directly determined by the octahedral oxygen coordination, which takes into account that the 8*a* Wyckoff position is tetrahedrally coordinated, while the 16*c* position is octahedrally coordinated.

However, this visual determination of lifetimes does not always allow for a clear distinction between t_{16c} and t_{path}. Therefore, we assume that lifetimes of the 8*a*↔8*a* diffusion step vary by ± 12 fs, which corresponds to ± 6 time steps. For the 8*a*↔16*c* diffusion step, the determination is somewhat simpler because the 16*c* lifetime t_{16c} is directly related to the plateau of $\mathrm{F}_x[i][t]$, see Figs. 2c) and e). In contrast, t_{path} can be determined directly from the initial and final areas of the plateau, see Figs. 2c) and e). The lifetimes obtained in this way vary by ± 4 fs, which corresponds to ± 2 time steps. Determining of the 16*c* lifetime for the 8*a*↔16*d* diffusion step is difficult. In this step the Li ion passes through both the 16*c* and the 48*f* Wyckoff positions. Therefore, the 16*c*-lifetime can only be determined by the octahedral oxygen coordination approach and not by the $\mathrm{F}_x[i][t]$ function. Analogous to the 8*a*↔8*a* diffusion step the lifetimes vary by ± 12 fs, corresponding to ± 6 time steps.

As an alternative to the presented procedure for determining the lifetime τ, this could also be done using an autocorrelation function, as demonstrated by M. Campetella *et al*.[1] However, the presented approach represents alternative that allows to directly calculate the lifetimes τ, which is composed of different contributions. Therefore the τ_{16c} lifetime can be calculated direclty by this approach.

Overall, the determination of the t_{16c} lifetime is not trivial and the obtained values vary slightly by a few time steps/fs. This is especially true when the octahedral oxygen coordination approach is used to determine t_{16c}. The fluctuation values are based on the results obtained and have therefore been chosen arbitrarily to some extent. However, we assume that the obtained lifetimes are accurate within a small variation. By combining both approaches, the Li vacancy diffusion steps were characterized in this study. With the combined procedure, the location of the Li vacancies can be determined for each simulation time step.

S2: Characterization of Li vacancy diffusion at simulation temperatures of 800 K – 950K

a) Number of diffusion steps for the three Li vacancies

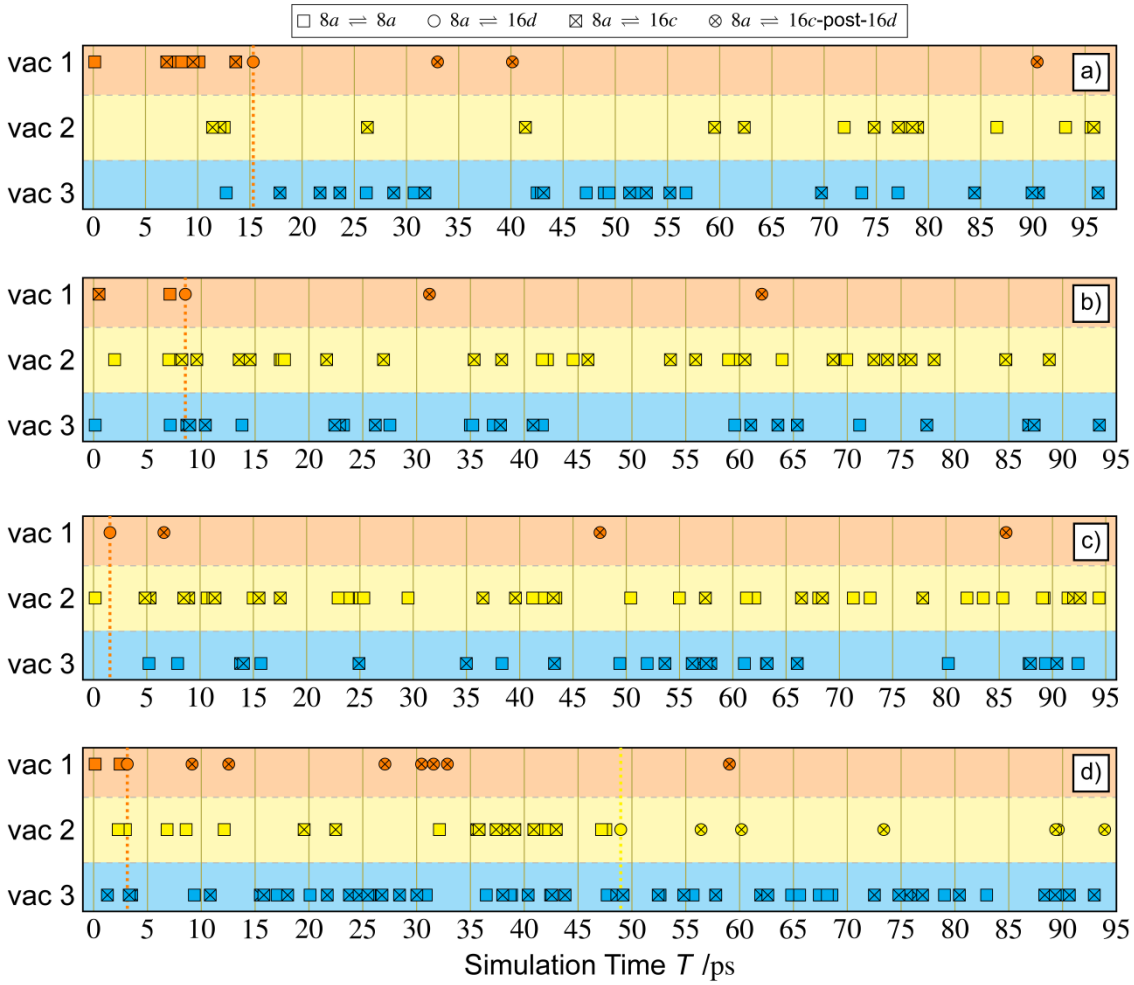

Figure S2: Number and type of the different diffusion steps (8*a*↔8*a*, 8*a*↔16*d* and 8*a*↔16*c*) plotted against the simulation time of the FPMD simulation for each of the three Li vacancies at a simulation temperature of a) 800 K, b) 850 K, c) 900 K and d) 950 K. Color code: orange: Li vacancy 1 (vac 1); yellow: Li vacancy 2 (vac 2) and blue: Li vacancy 3 (vac 3). Circle with cross inside indicates the 8a↔16c diffusion steps that occurs after the Li vacancy is trapped at a 16*d* Wyckoff position.

Table S1: Absolut and normalized (to 100 ps simulation time) number of the three diffusion steps (8*a*↔16*d*, 8*a*↔8*a* and 8*a*↔16*c*), and the total number of all diffusion steps as a function of the simulation temperature.

Simulation temperature	**absolute number of diffusion steps**				**norm. number of diffusion steps to 100 ps simulation time**			
	8*a*↔16*d*	**8*a*↔8*a***	**8*a*↔16*c***	**Σ**	**8*a*↔16*d***	**8*a*↔8*a***	**8*a*↔16*c***	**Σ**
800 K	1	23	27 (+3)	54	1	23	27 (+3)	54
850 K	1	25	39 (+2)	67	1	27	41 (+2)	71
900 K	1	41	31 (+3)	76	1	44	33 (+3)	81
950 K	2	34	48 (+13)	97	2	36	51 (+13)	102
1000 K	2	19	34 (+15)	70	2	25	45 (+20)	92

() the additional 8*a*↔16*c*-post-16*d* steps, which are carried out by a Li vacancy after it is trapped on a 16*d*

Table S2: Absolute numbers of the three diffusion steps (8*a*↔16*d*, 8*a*↔8*a* and 8*a*↔16*c*) and the $8a \leftrightarrow 16c/8a \leftrightarrow 8a$-ratio as a function of the Li vacancy (vac 1, vac 2 and vac 3) as well as a function of the simulation temperature. The $8a \leftrightarrow 16c/8a \leftrightarrow 8a$-ratio indicates that every $8a \leftrightarrow 8a$ step is followed by $x \cdot (8a \leftrightarrow 16c)$ steps.

Simulation temperature	vac 1				vac 2				vac 3			
	8*a*↔16*d*	**8*a*↔8*a***	**8*a*↔16*c***	**$\frac{8a\leftrightarrow16c}{8a\leftrightarrow8a}$ ratio***	**8*a*↔16*d***	**8*a*↔8*a***	**8*a*↔16*c***	**$\frac{8a\leftrightarrow16c}{8a\leftrightarrow8a}$ ratio***	**8*a*↔16*d***	**8*a*↔8*a***	**8*a*↔16*c***	**$\frac{8a\leftrightarrow16c}{8a\leftrightarrow8a}$ ratio***
800 K	1	4	11 (+3)	-/-	0	13	13	1	0	6	3	0.5
850 K	1	1	2 (+1)	-/-	0	12	22	1.69	0	12	16	1.33
900 K	1	1	0 (+3)	-/-	0	28	16	0.57	0	12	15	1.25
950 K	1	3	0 (+7)	-/-	1	10	9 +(6)	-/-	0	21	39	1.86
1000 K	1	1	3 (+7)	-/-	1	2	7 +(8)	-/-	0	16	24	1.5

() the additional 8*a*↔16*c*-post-16*d* steps, which are carried out by a Li vacancy after it is trapped on a 16*d*

* 8*a*↔16*c*-post-16*d* diffusion steps are not included in the calculation

-/- no reliable analysis is possible as the Li vacancies migrate after a short period of time to a 16*d* position

b) Lifetime of the 16*c* transition site

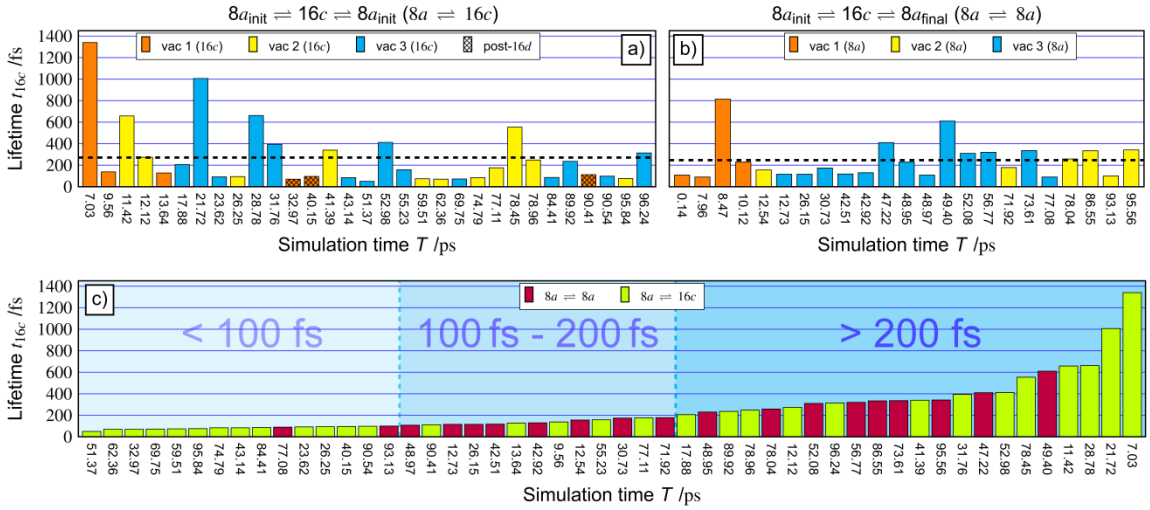

Figure S3: Lifetimes t_{16c} of the 16*c* transition sites during the 800 K FPMD simulation. The 16*c* lifetime is plotted for each of the three Li vacancies in a) for the 8*a*↔16*c* diffusion step and in b) for the 8*a*↔8*a* diffusion step. Shaded bars in a) indicate the 16*c* lifetimes for the 8*a*↔16*c* diffusion steps that occur after the respective Li vacancy is trapped in a 16*d* Wyckoff position. Black dotted line in a) and b) indicates the mean lifetime of the 16*c* transition site during a) the 8*a*↔16*c* and b) 8*a*↔8*a* diffusion steps. c) Representation of the increasing 16*c* lifetime includes the 8*a*↔8*a* and 8*a*↔16*c* diffusion steps, which contains the data from the two previous plots a) and b) without the Li vacancy assignment.

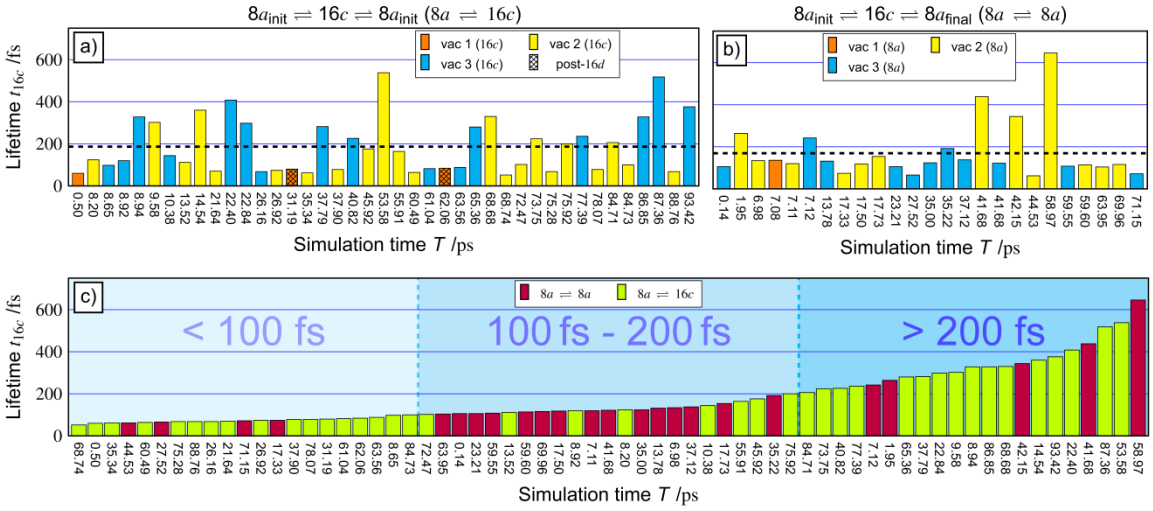

Figure S4: Lifetimes t_{16c} of the 16*c* transition sites during the 850 K FPMD simulation. The 16*c* lifetime is plotted for each of the three Li vacancies in a) for the 8*a*↔16*c* diffusion step and in b) for the 8*a*↔8*a* diffusion step. Shaded bars in a) indicate the 16*c* lifetimes for the 8*a*↔16*c* diffusion steps that occur after the respective Li vacancy is trapped in a 16*d* Wyckoff position. Black dotted line in a) and b) indicates the mean lifetime of the 16*c* transition site during a) the 8*a*↔16*c* and b) 8*a*↔8*a* diffusion steps. c) Representation of the increasing 16*c* lifetime includes the 8*a*↔8*a* and 8*a*↔16*c* diffusion steps, which contains the data from the two previous plots a) and b) without the Li vacancy assignment.

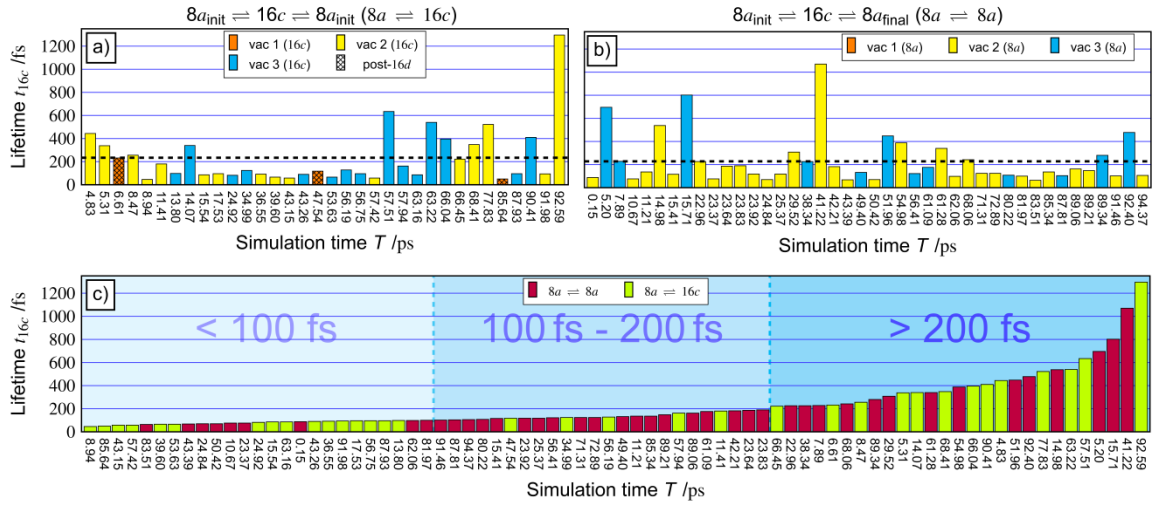

Figure S5: Lifetimes t_{16c} of the 16*c* transition sites during the 900 K FPMD simulation. The 16*c* lifetime is plotted for each of the three Li vacancies in a) for the 8*a*↔16*c* diffusion step and in b) for the 8*a*↔8*a* diffusion step. Shaded bars in a) indicate the 16*c* lifetimes for the 8*a*↔16*c* diffusion steps that occur after the respective Li vacancy is trapped in a 16*d* Wyckoff position. Black dotted line in a) and b) indicates the mean lifetime of the 16*c* transition site during a) the 8*a*↔16*c* and b) 8*a*↔8*a* diffusion steps. c) Representation of the increasing 16*c* lifetime includes the 8*a*↔8*a* and 8*a*↔16*c* diffusion steps, which contains the data from the two previous plots a) and b) without the Li vacancy assignment.

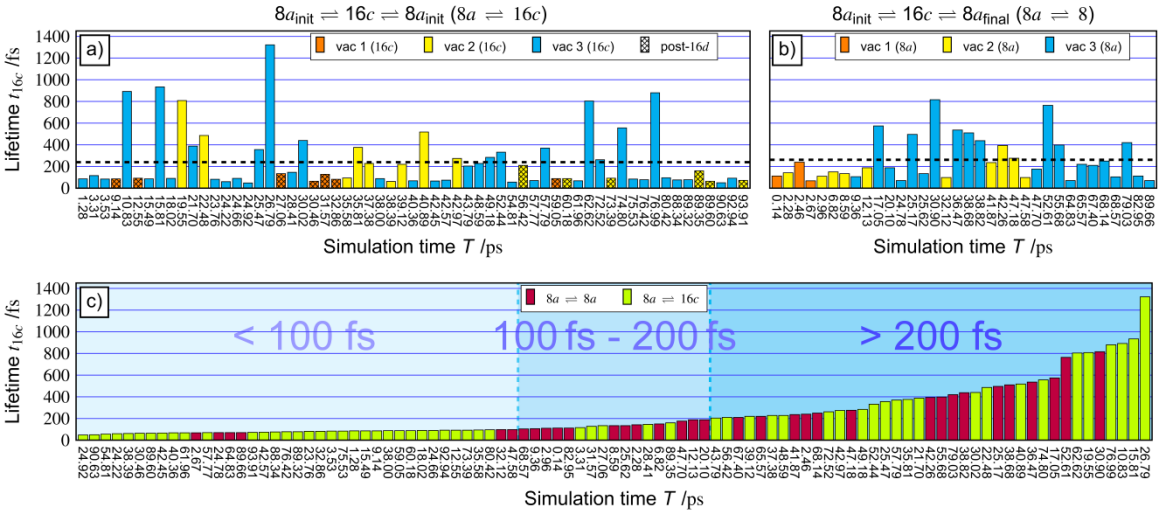

Figure S6: Lifetimes t_{16c} of the 16*c* transition sites during the 950 K FPMD simulation. The 16*c* lifetime is plotted for each of the three Li vacancies in a) for the 8*a*↔16*c* diffusion step and in b) for the 8*a*↔8*a* diffusion step. Shaded bars in a) indicate the 16*c* lifetimes for the 8*a*↔16*c* diffusion steps that occur after the respective Li vacancy is trapped in a 16*d* Wyckoff position. Black dotted line in a) and b) indicates the mean lifetime of the 16*c* transition site during a) the 8*a*↔16*c* and b) 8*a*↔8*a* diffusion steps. c) Representation of the increasing 16*c* lifetime includes the 8*a*↔8*a* and 8*a*↔16*c* diffusion steps, which contains the data from the two previous plots a) and b) without the Li vacancy assignment.

Table S3: Absolute and normalized (to 100 ps simulation time) probabilities that a 8*a*↔8*a* or 8*a*↔16*c* diffusion step takes place within a 16*c* lifetime ranges of $t_{16c} < 100$ fs, $100\text{ fs} \leq t_{16c} < 200$ fs and $t_{16c} \geq 200$ fs. In addition, the absolute mean 16c lifetime t_{mean} within the 8*a*↔8*a* and 8*a*↔16*c* diffusion step is given

	absolute 16*c* life times								**normalized 16*c* life times to 100 ps simulation time**					
	$t_{16c} <$ 100 fs /%		100 fs $\leq t_{16c} <$ 200 fs /%		$t_{16c} \geq$ 200 fs /%		t_{mean} /fs		$t_{16c} <$ 100 fs /%		100 fs $\leq t_{16c} <$ 200 fs /%		$t_{16c} \geq$ 200 fs /%	
Simulation temperature	**8*a*↔8*a***	**8*a*↔16*c***	**8*a*↔8*a***	**8*a*↔16*c***	**8*a*↔8*a***	**8*a*↔16*c***	**8*a*↔8*a***	**8*a*↔16*c***	**8*a*↔8*a***	**8*a*↔16*c***	**8*a*↔8*a***	**8*a*↔16*c***	**8*a*↔8*a***	**8*a*↔16*c***
800 K	13	87	67	33	46	54	247	271	13	87	67	33	46	54
850 K	20	80	67	33	23	77	169	187	19	81	68	32	22	78
900 K	33	67	80	20	52	48	228	234	32	68	81	19	52	48
950 K	15	84	71	29	41	59	262	240	15	85	72	28	42	58
1000 K	4	96	70	30	17	83	266	265	3	97	70	30	16	84

S3: Temperature dependence of the 8*a*↔16*c*-post-16*d* steps

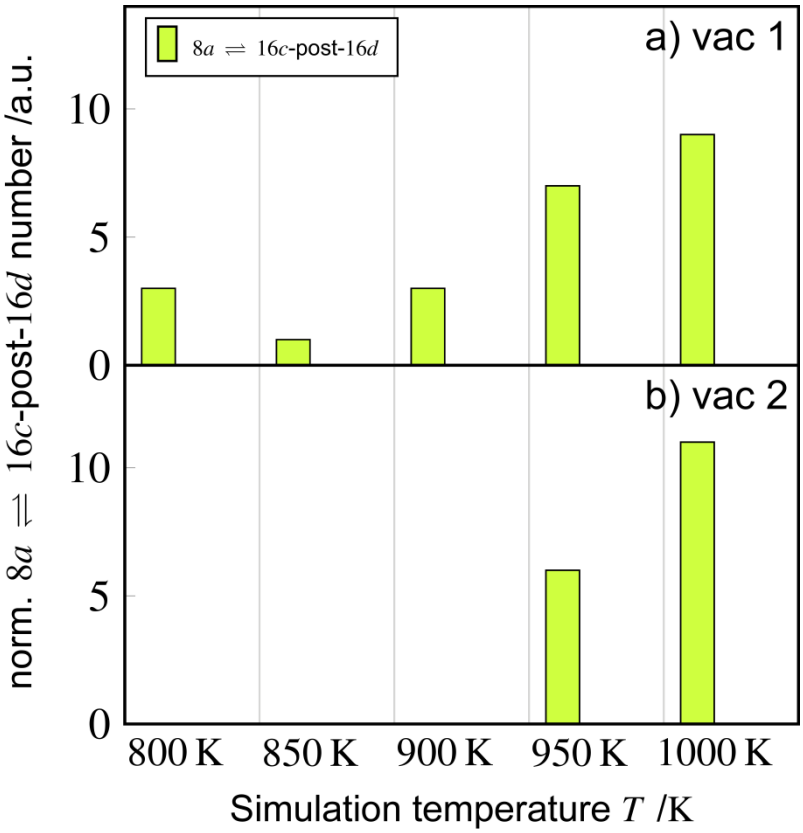

Figure S7: Temperature dependence of the normalized 8*a*↔16*c*-post-16*d* diffusion step number for the Li vacancy a) vac 1 and b) vac 2. As vac 2 is only trapped in a 16*d* position above 950 K, there is no data available for 8*a*↔16*c*-post-16*d* in the temperature range of 800 K to 900 K.

S4: Determining self-diffusion coefficient $D_{\mathrm{self}}(T)$ and jump frequency $\Gamma(T)$ in the temperature range of 800 K to 1000 K

Table 4: Calculated self-diffusion coefficients $D_{\mathrm{self}}(T)$ and jump frequency $\Gamma(T)$ for Li vacancy diffusion in LTO in the temperature range of 800 K to 1000 K.

Simulation temperature /K	Self-diffusion coefficient $D_{\mathrm{self}}(T)$ /cm^2/s	Jump frequency $\Gamma(T)$ /GHz
800	$1.06 \cdot 10^{-5}$	4.69
850	$1.23 \cdot 10^{-5}$	5.47
900	$1.78 \cdot 10^{-5}$	7.91
950	$1.81 \cdot 10^{-5}$	8.05
1000	$3.09 \cdot 10^{-5}$	13.72

S5: Mean square displacement for the FPMD simulation at 1000 K to determine the temperature independent diffusion coefficient D_0 and the activation energy E_A

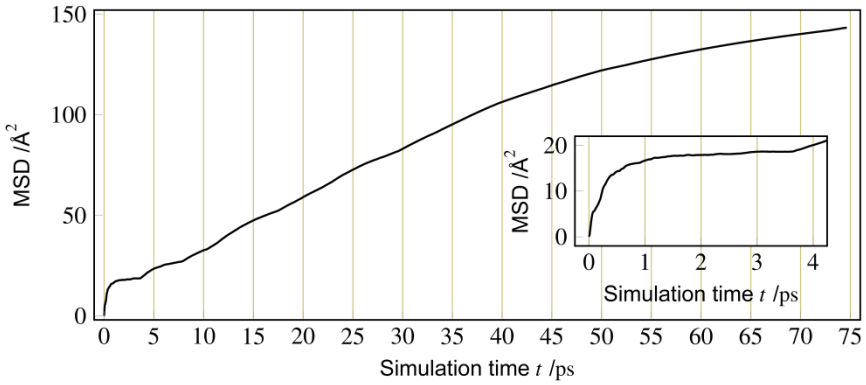

Figure S8: Mean square displacement (MSD) for the FPMD simulation at 1000 K, as well as zoomed region around the ballistic motion/error.

References

(1) Campetella, M.; Macchiagodena, M.; Gontrani, L.; Kirchner, B. Effect of alkyl chain length in protic ionic liquids: an AIMD perspective. *Molecular Physics* **2017**, *115*, 1582–1589.